Tomography-assisted control for the microwave drying process of polymer foams

Marzieh Hosseini [a,*], Anna Kaasinen [a], Guido Link [b], Mahdi Aliyari Shoorehdeli [c], Timo Lähivaara [a], Marko Vauhkonen [a]

[a] Department of Applied Physics, University of Eastern Finland, Kuopio, Finland
[b] Institute for Pulsed Power and Microwave Technology, Karlsruhe Institute of Technology, Karlsruhe, Germany
[c] Mechatronics Department, Electrical Engineering Faculty, K.N. Toosi University of Technology, Tehran, Iran

ARTICLE INFO

ABSTRACT

This paper presents the integration of electrical capacitance tomography (ECT) with a moisture controller for the microwave drying of polymer foam. The proportional–integral (PI) control and the linear quadratic Gaussian (LQG) control are employed in designing the controller. The control objective in this process is that the moisture of polymer foam after the drying process reaches the desired set point. The permittivity distribution of polymer foam after the drying process is estimated in real-time using a designed ECT sensor and transferred as feedback to the controller. Since the permittivity and the moisture are strongly correlated, the material moisture can be controlled by controlling the permittivity. A state-space model is derived for the microwave drying process based on a system identification approach using the experimental data from the process. The derived model is employed in designing the LQG controller and adjusting the parameters of the PI controller. The designed controllers are implemented on a testbed microwave oven, and the experimental results show that the designed controllers are able to follow the desired set point moisture. The performance of the system with both controllers is compared, and their advantages and disadvantages are discussed. Moreover, the benefits of having a moisture controller for the microwave drying process are shown in simulation studies compared to an uncontrolled system.

1. Introduction

High-power microwave (MW) drying has a wide application in drying porous materials. With the advantages of volumetric heating, saving energy, and processing time, the microwave drying technology is reported to be at least twice as effective as the other methods [1]. The wet material enters the oven cavity, where several magnetrons act as the sources of microwave heating energy and result in the fast evaporation of moisture in the wet material.

The quality of the material after the drying process highly depends on the moisture content and the moisture homogeneity of the material [2]. The microwave drying process aims to result in a specific amount of moisture after drying, depending on the material and the application [3]. Furthermore, the remaining moisture in the material should be as homogeneous as possi-

ble [4]. Designing a moisture controller can help to monitor the material moisture and adjust the power level of the magnetrons to reach the desired moisture, and ensure the homogeneity of the moisture distribution by selective heating.

The application of a moisture controller in continuous microwave drying has not been studied so far since there are no suitable methods applied to measure moisture content/distribution in a continuous microwave drying process. The standard method to measure the moisture in microwave drying is by measuring the weight of the sample [5–8]. In Li et al. [9], the drying rate of the sample was measured using a digital balance connected to the sample, and the drying temperature was adjusted proportionally using a pre-defined strategy. Measuring the sample weight is suitable for the control of batch microwave ovens. However, this method cannot be applied in a continuous microwave drying process where the wet material is constantly moving. Moreover, weighting the material provides only the average moisture value and not its distribution.

Most of the feedback controllers designed for the microwave oven in both drying and heating processes are temperature controllers since the material temperature is readily available through the infrared (IR) cameras or the fiber-optics probes [10–14]. In

* Corresponding author.
E-mail addresses: marzieh.hosseini@uef.fi (M. Hosseini), anna.kaasinen@uef.fi (A. Kaasinen), guido.link@kit.edu (G. Link), aliyari@kntu.ac.ir (M. Aliyari Shoorehdeli), timo.lahivaara@uef.fi (T. Lähivaara), marko.vauhkonen@uef.fi (M. Vauhkonen).

Cuccurullo et al. [10], the instantaneous hot spot among apple samples was detected using an IR camera, and an on–off control on a constant delivered power was proposed to keep the desired temperature. Furthermore, the process was coded to stop when a pre-defined moisture value was achieved. Temperature and power control are also discussed in [14] for a microwave drying process. Four drying modes were discussed, where the temperature and power were controlled in different suggested drying modes based on pre-defined profiles. However, temperature control can only prevent undesired hot spots and prevent damaging the material. In order to achieve the desired moisture inside the material and ensure a homogeneous moisture distribution, a moisture controller is required.

This research proposes a novel idea of integrating electrical capacitance tomography (ECT) with control for the microwave drying process. Although tomographic imaging techniques, in general, have established their unique roles in monitoring different industrial processes, their combination with control has only been studied in very few applications [15,16].

The investigated application in this study is drying wet polymer foam after the impregnation phase in the thermal insulation industry. The polymer foam is dipped into water and chemicals to generate predetermined features in foam. After the impregnation, the wet foam enters the microwave oven on the conveyor belt and passes through the oven cavity to dry. The main goal in this process is to achieve the desired moisture (e.g., 10%–20% on a wet basis) inside the foam. Moreover, the remaining moisture should be as homogeneous as possible.

An ECT sensor is designed and installed at the output of the microwave oven to estimate the permittivity distribution of the polymer foams after the drying process. Generally, the ECT sensor is a contactless, fast and reliable method to estimate the moisture distribution of dielectric materials [17–20]. In ECT, the inter-electrode capacitances between the electrodes surrounding a target material (foam in this study) are measured, and the permittivity distribution of the material is estimated using a reconstruction algorithm. To the best of our knowledge, the designed ECT sensor in this research is the first proposed sensor in the literature to monitor the moisture distribution in a continuous drying process in practice. Due to the application-specific requirements, the proposed ECT sensor has a wide rectangular structure, unlike standard ECT sensors. The unusual sensor shape resulted in a weak measurement signal and a challenging reconstructions process. The sensor provides two-dimensional (2D) cross-sectional images from the permittivity distribution in real-time, which shows the moisture locations in the foam and the permittivity change in those locations. The moisture distribution of the foam can then be estimated through a calibration map [21]. However, to avoid calibration errors, the permittivity estimate is directly sent to a designed moisture controller.

The moisture controller is designed with two different methods for the microwave drying process to achieve the desired moisture inside the polymer foams after the drying process. The first designed controller is a proportional–integral (PI) controller, and the second controller is based on the linear quadratic Gaussian (LQG) control method. Since the microwave drying process is a complicated system with several actuators (the magnetrons), the designed controllers in the first step are assumed to be single-input single-output (SISO) to simplify the problem. The power level of magnetrons is determined altogether to satisfy a desired average permittivity in the 2D cross-section of the foam after the drying process. Since the ECT can also estimate the permittivity distribution, a multi-input multi-output (MIMO) controller can be designed in future studies as the next step to ensure the homogeneity of the dried foam.

Designing a model-based controller like the LQG controller requires a mathematical model of the process. Moreover, having a model can help to adjust the parameters of non-model-based controllers such as PI controllers. Modeling the microwave drying process with coupled heat and moisture transfer is a difficult task. There are several studies on multi-physics models of a microwave drying process [22,23]. However, they are expensive and time-consuming to compute, so they are not suitable for real-time closed-loop control.

A system identification approach with an insight into the physics behind the process is adopted in this research to find a state-space model of the microwave drying process using the ECT measurements. The main challenge in modeling the studied microwave drying process is that the ECT sensor is located at the end of the process, and there is no information of the foam moisture during the relatively long traveling time inside the oven. This challenge was addressed by introducing a virtual input and dividing the system into two subsystems. The derived model for the whole process is SISO with the power level of the magnetrons as its input and the average permittivity change of the dried foam as its output. The obtained model is used to design the LQG controller and determine the PI controller parameters.

The content of this paper is structured as follows. The main principles of the ECT sensor and its design are given in Section 2. In Section 3, the microwave drying process is explained, and the process modeling is discussed. The design procedure of the PI and LQG controllers is described in Section 4, and the results and discussion are covered in Section 5. Section 6 summarizes this research and gives the conclusion.

2. Electrical capacitance tomography

Designing a moisture controller requires information on material moisture during the process. In continuous microwave drying, where the wet material is moving on a conveyor belt, conventional methods such as measuring the weight of the material are impossible to use. The ECT sensor is an attractive tool for estimating and monitoring moisture distribution since it is contactless, fast, and inexpensive. Electrical capacitance tomography is an imaging modality to reconstruct the material permittivity distribution. Since the permittivity is strongly correlated with the moisture, the reconstructed permittivity can be used in estimating the moisture distribution.

The ECT sensor consists of several measuring electrodes mounted on a frame around an imaging area where the target material is inserted, as shown in Fig. 1. Additionally, electrically grounded guard electrodes are placed between the adjacent measuring electrodes to increase the sensitivity of measurements; however, they do not play a role in the measurement procedure. The measurement starts by exiting one of the electrodes while the rest are grounded, and the electrical capacitances between the exited electrode and other measuring electrodes are recorded. The same measurements are repeated by exciting every measuring electrode until a complete set of measurements is collected. Assuming N measuring electrodes around the imagining area, $m = N(N-1)/2$ independent measurements are collected in each frame of measurements. The collected data are used in a reconstruction algorithm to estimate the material 2D permittivity distribution.

Reconstructing the permittivity distribution of the material based on the collected measurements is a so-called inverse problem. In this research, the difference imaging method was chosen to solve the inverse problem as this method is linear and fast to compute, making it one of the best candidates for a real-time application [24,25]. In this method, two sets of measurements are collected: the reference data (C_{ref}), which are the capacitance measurements while a dry foam is inside the sensor, and the measurement data (C_M), which are the capacitance measurements
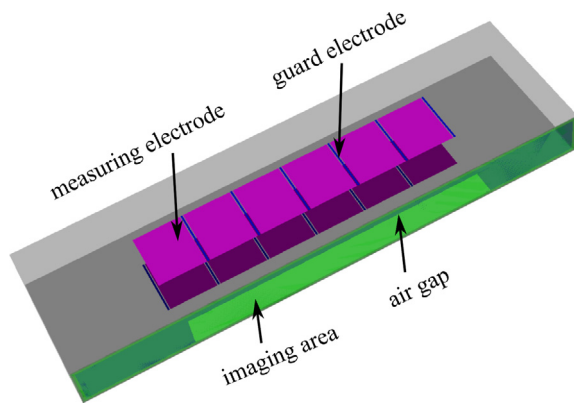
Fig. 1. The ECT sensor illustration with six measuring electrodes on the top surface and another six measuring electrodes on the bottom surface of the sensor. An electrically grounded guard electrode is located between adjacent measuring electrodes. An air gap is left between the imaging area and the top surface electrodes to allow foam movement.

while a wet material is inside the sensor. The change in the permittivity distribution of the wet material compared to the dry material can then be estimated as

$$\Delta\epsilon = \epsilon - \epsilon_{\text{ref}} = H\left(C_M - C_{\text{ref}}\right),\tag{1}$$

where ϵ is the permittivity distribution of the wet material, ϵ_{ref} is the dry foam permittivity, and H is the reconstruction matrix. More detailed descriptions can be found in [21].

Although the ECT sensors have the same main principles, each sensor should still be designed based on the specific requirements of their application. The target material in this study was polymer foam with a width of 49.3 cm, a thickness of 3 cm, and a long length, continuously moving on a conveyor belt. These specifications required a sensor design that has a rectangular structure, unlike common ECT sensors that have a round shape. An electrode plane with six measuring electrodes was mounted on the top surface of the sensor, while another six measuring electrodes were mounted on the bottom surface of the sensor. There was an air gap of 1 cm between the foam and the top surface electrodes to allow easy movement of the polymer foam. The bottom surface electrodes were located under the thin conveyor belt that carried the polymer foam. There were no electrodes mounted on the sensor sides as they did not significantly contribute to the measurements and the reconstructions. Fig. 1 shows the designed ECT sensor and its 12 electrodes.

The sensor dimension was 87 cm × 25 cm × 4 cm. The wide frame of the ECT sensor and its rectangular cross-section resulted in a considerable distance between the non-neighboring electrodes and a small measurement signal between them. Using wide electrodes in the sensor design helped to compensate for the small measurement signal. The measuring electrodes on the top and bottom surfaces of the sensor had an area of 10 cm × 8.1 cm. The guard electrodes inserted between the measuring electrodes had a size of 10 cm × 0.3 cm. The ECT sensor based on this design was built and installed at the exit of the testbed microwave oven in this research. Fig. 2(a) shows the built ECT sensor while estimating the permittivity distribution of a moving foam. A picture from the inside surface of the sensor (bottom plate) is shown in Fig. 2(b). Six measuring electrodes and the guard electrodes between them can be seen on the bottom surface.
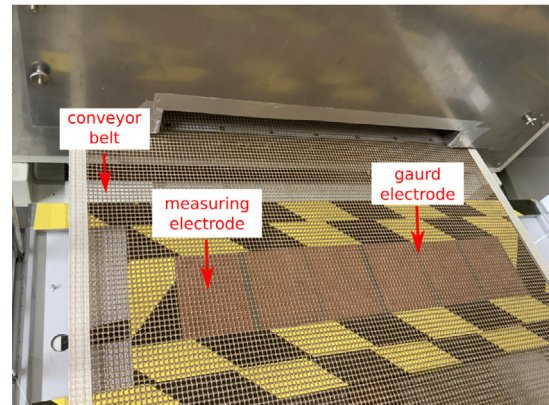
3. Microwave drying process

3.1. Drying process of polymer foam

Microwave ovens can be built as batch or continuous (conveyor-belt) ovens. In a batch oven, the wet material is exposed to
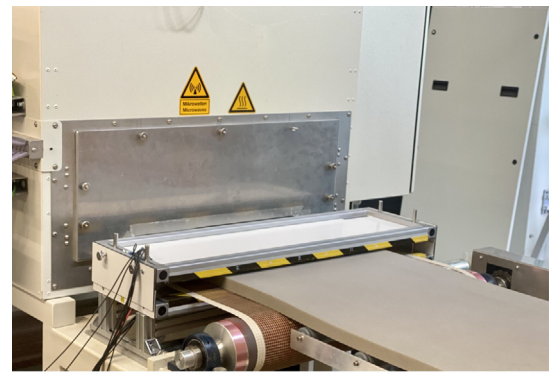
(a)

(b)

Fig. 2. The designed and built ECT sensor. **(a):** The ECT sensor while estimating the permittivity of a moving polymer foam. **(b):** The bottom electrode plane of the ECT sensor installed under the conveyor belt.

Fig. 3. Illustration of the continuous oven HEPHAISTOS with three modules, placed at the Karlsruhe Institute of Technology, Germany.

microwave heating for a specific time in a closed oven, while in a continuous oven, a conveyor belt moves through an open oven carrying the wet material to get dried. Fig. 3 shows an illustration of the continuous microwave oven studied in this research, called HEPHAISTOS, located at Karlsruhe Institute Technology, Germany. This system is a combination oven with circulating hot air that removes the evaporated moisture. The total length of the oven is 729 cm, and it includes three modules, each equipped with six magnetrons as the heating source. The magnetrons work with a frequency of 2.45 GHz and a maximum power of 2 kW, which gives a total maximum power of 36 kW for the whole oven.

One of the applications of the continuous microwave oven in the industry is to dry polymer foams after the impregnation process. Impregnation is a chemical process that generates new
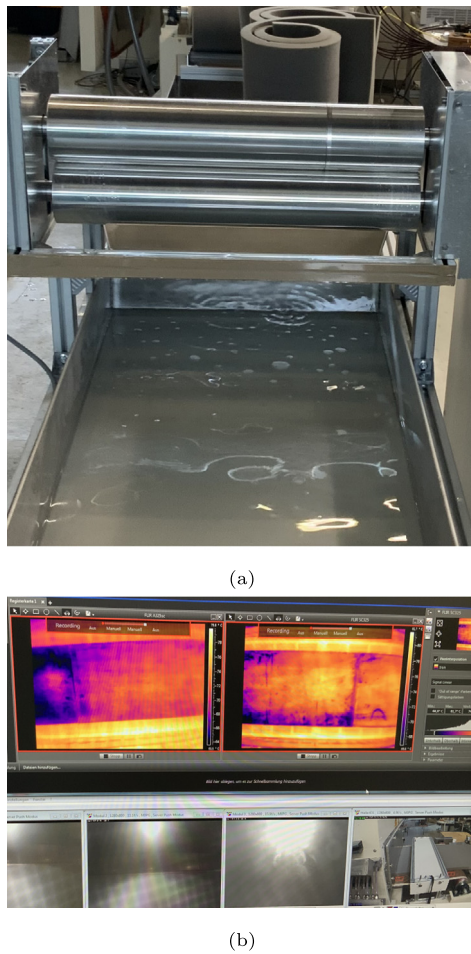
(a)

(b)

Fig. 4. (a): The impregnation tub with two rotating bars to ensure a homogeneous initial moisture. **(b):** The images from the IR cameras installed inside the oven.

features in polymer foams suitable for insulation applications in the construction industry. The polymer foam first moves into an impregnation tub filled with water and chemicals, shown in Fig. 4(a). The foam then passes through two rotating bars that squeeze out the excess water from the foam to save time and energy during the drying process and make the moisture inside the foam more homogeneous. The wet polymer foam enters the oven on a conveyor belt to pass through all three modules and dry.

During the process, only the surface temperature of the foam can be monitored using IR cameras, and there is no information available on the moisture. Fig. 4(b) shows the IR images transmitted by the IR cameras installed inside each module. In this study, the ECT sensor is installed after the last microwave module, as shown in Fig. 2, to estimate the material permittivity (moisture) after the drying process.

3.2. Process modeling

Model-based controllers require a mathematical model of the process. Furthermore, having a model of the process helps to simulate the system behavior in different conditions and evaluate the performance of the designed controllers before implementing them on the system. However, the microwave drying process is a complex process involving coupled electromagnetics and simultaneous heat and moisture transfer. These types of systems are typically described with partial differential equations (PDEs), depending both on time and position, and are so-called distributed parameter systems (DPS).

In our earlier study [23], the coupled PDEs for heat and moisture transfer proposed by Luikov [26,27] were modified and employed to model one of the oven modules with a length of 50 cm while the actual length of each module is 100 cm. Modeling the whole process with three modules is far more complex and time-consuming. Moreover, the exact parameters of the heat and moisture transfer model are not available for the polymer foams. These limitations embarked on employing the system identification methods in which the precise physical knowledge of the process was no longer required.

System identification is a methodology of analyzing collected input and output information from the process by giving specific inputs to the system and measuring the corresponding outputs [28,29]. A mathematical model (linear or nonlinear) can be derived based on the collected information. In this study, the aim was to control the output foam permittivity by adjusting the power level of the magnetrons. Therefore, a series of experiments were conducted to collect sufficient input–output data to find a SISO model of the process.

The power level of the magnetrons (percentage of the maximum power), P, was the system input, such that $0 \leq P \leq 100$. Since the goal was to obtain a single-input model, all 18 magnetrons were synchronized together, and one input was given to all of them during the whole experiments so that $P_l = P$, $l = 1, \ldots, 18$, where P_l is the power level of the lth magnetron. The initial foam moisture percentage before the drying process, M_{in}, also affects the system output. Therefore, the variation of the initial moisture, ΔM_{in} was taken as the input disturbance to the process, computed as

$$\Delta M_{\text{in}} = M_{\text{in}} - M_{\text{avg}}, \tag{2}$$

where M_{avg} is the average initial moisture of the foam. The ECT sensor estimated the permittivity change distribution of the 2D cross-section of the foam, $\Delta\epsilon$, while the foam was passing through the ECT sensor. The average value of this 2D distribution was converted to a wet-basis value and taken as the system output. The wet-basis average permittivity change, $\Delta\epsilon_{\text{w}}$, can be computed as

$$\Delta\epsilon_{\text{d}} = \frac{\overline{\Delta\epsilon}}{\epsilon_{\text{ref}}} \times 100, \tag{3}$$

$$\Delta\epsilon_{\text{w}} = \frac{\Delta\epsilon_{\text{d}}}{100 + \Delta\epsilon_{\text{d}}} \times 100, \tag{4}$$

where $\Delta\epsilon_{\text{d}}$ is the dry basis permittivity change (in percentage), $\overline{\Delta\epsilon}$ is the average value of $\Delta\epsilon$ at the n nodes of the 2D discretization mesh, and ϵ_{ref} is the dry foam permittivity. Note that $\Delta\epsilon_{\text{w}}$ is correlated with the foam average moisture after the drying process through a calibration map [21]. Therefore the average moisture of the output foam can be controlled by controlling $\Delta\epsilon_{\text{w}}$.

Different experiments were conducted to collect input–output data of the system. The test materials in these experiments were multiple polymer foam sheets as it was not practical to use a long enough foam that could run through the experiment for several hours. Standard inputs, including a pseudorandom binary sequence (PRBS) signal and an amplitude-modulated pseudorandom binary sequence (APRBS), were given as the pre-specified power levels to the magnetrons and the corresponding measurements from the ECT sensor were collected. Fig. 5 shows a schematic of the continuous experiment where the foam sheets were placed next to each other with no gap and sent to the microwave oven on a conveyor belt with a speed of 40 cm/min. The travel time for each point of the foam from entering the oven to reaching the middle of the ECT sensor was 1129 s.
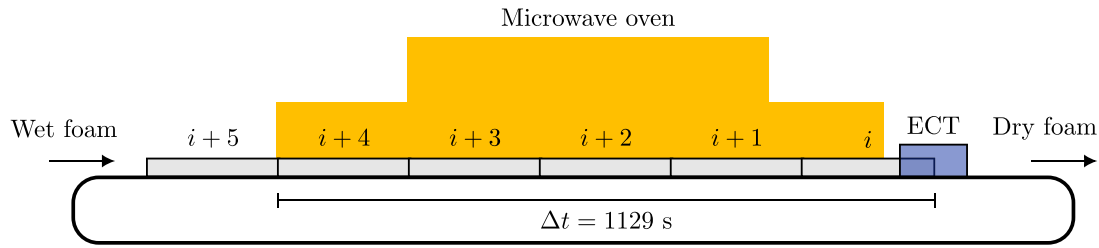
Fig. 5. The schematic of the experimental procedure in collecting input–output data of the microwave drying process. The polymer foam sheets are shown with gray rectangles, which move on a conveyor belt through the oven and the ECT sensor.
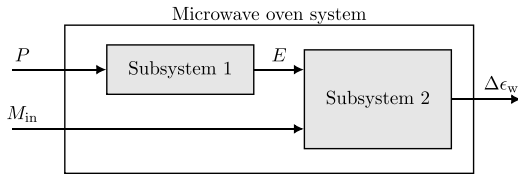

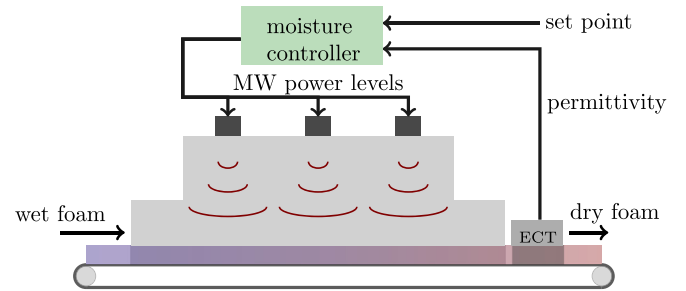**Fig. 6.** Dividing the microwave oven system into two subsystems.

Fig. 7. A schematic of the closed-loop microwave drying process. The reconstructed permittivity from the ECT sensor measurements is sent to the controller, and the controller adjusts the power level of the magnetrons based on the received information.

One of the main challenges in the modeling process was the ECT sensor location. As shown in Fig. 5, from the moment the foam enters the oven cavity until it reaches the ECT sensor, it takes almost 20 min (1129 s). Therefore, the immediate effect of changing the power levels on the moisture distribution of the foam during the drying process could not be observed in the final measurements. Hence, based on the physical knowledge about the system, a new virtual input $E(t)$ was introduced as the overall applied energy to each location of the foam before it reaches the ECT electrode plane. This input was calculated as the integral of the applied power over the time interval that the foam spent in the cavity. This way, the process was divided into two subsystems in series, as shown in Fig. 6.

In the first experiment, a PRBS signal was given as the input to the magnetrons. The dataset collected with this input signal was used as the training dataset to estimate the parameters of a model for the microwave drying process. The state-space model structure was chosen for modeling as the state-space model is a pre-requirement for many model-based control methods. More details on the data processing and modeling procedure are given in [30]. The derived model was in discrete space with a sample time of $T_s = 1$ s and can be described as

$$\boldsymbol{x}[k+1] = \boldsymbol{A}\boldsymbol{x}[k] + \boldsymbol{B}_1\boldsymbol{u}[k - T_{d1}] + \boldsymbol{B}_2\boldsymbol{w}[k - T_{d2}], \tag{5}$$

$$\boldsymbol{y}[k] = \boldsymbol{C}\boldsymbol{x}[k], \tag{6}$$

where $\boldsymbol{x}[k] \in \mathbb{R}^{8 \times 1}$ is the state vector, $\boldsymbol{u}[k] = P[k]$ is the control variable, $\boldsymbol{w}[k] = \Delta M_{in}[k]$ is the input disturbance, $\boldsymbol{y}[k] = \Delta\epsilon_w[k]$ is the process output, and the matrices $\boldsymbol{A} \in \mathbb{R}^{8 \times 8}$, $\boldsymbol{B}_1, \boldsymbol{B}_2 \in \mathbb{R}^{8 \times 1}$, and $\boldsymbol{C} \in \mathbb{R}^{1 \times 8}$ are the model parameters estimated using the MATLAB system identification toolbox given the collected inputs and output data. The input time delay for the control input is $T_{d1} = 261$ sampling periods, and for the input disturbance is $T_{d2} = 1129$ sampling periods.

The accuracy of the derived model should be evaluated using a different dataset called the validation dataset. The validation dataset was collected by giving an APRBS signal as the input to the magnetrons. The specifications of both PRBS and APRBS signals, such as pulse width and upper and lower limits, were chosen based on the knowledge of the process.

4. Controller design

The final aim of this research was to design a closed-loop moisture controller. Several control methods were investigated

using the model derived in Section 3.2. This paper presents the design procedure and experimental results from a PI controller and an LQG controller. The ECT sensor estimated the permittivity distribution of the polymer foam after exiting from the oven. Since the derived model was SISO, the average permittivity change was calculated using (4) and then sent to the designed moisture controller. The moisture controller receives the information from the ECT sensor along with a reference set point and calculates the command power levels given to the magnetrons. Fig. 7 shows a schematic of the microwave oven in connection with the moisture controller and the ECT sensor.

4.1. PI control

The PI controller is a standard industrial controller that has been found very efficient in most industrial applications. This controller was chosen as the first approach in this research as it is very efficient, cheap, and easy to implement. The derivative action in the PID controller family was not used here, and only a PI structure was employed since there was substantial environmental noise in the experiments done for this research due to possible microwave leakage. Furthermore, there were sometimes some drops of water at the ending surface of the foam, which created false error change.

Designing a PI controller does not require a process model. However, having a process model allowed us to analyze the step response of the process in simulation and tune the controller coefficients efficiently without conducting any experiments. Fig. 8 shows the step response of the derived model in Section 3.2. The model response to the step input of the control variable, $\boldsymbol{u}[k]$, is shown in Fig. 8(a), while Fig. 8(b) shows the step response to the input disturbance, $\boldsymbol{w}[k]$. The feedback PI controller is designed based on the step response of the control input. As shown in Fig. 8(a), the step response has a high rise time and settling time due to the time delay T_{d1}, but it is a stable system. The step response of the input disturbance can be used when designing a feedforward controller to reject the input disturbance. The
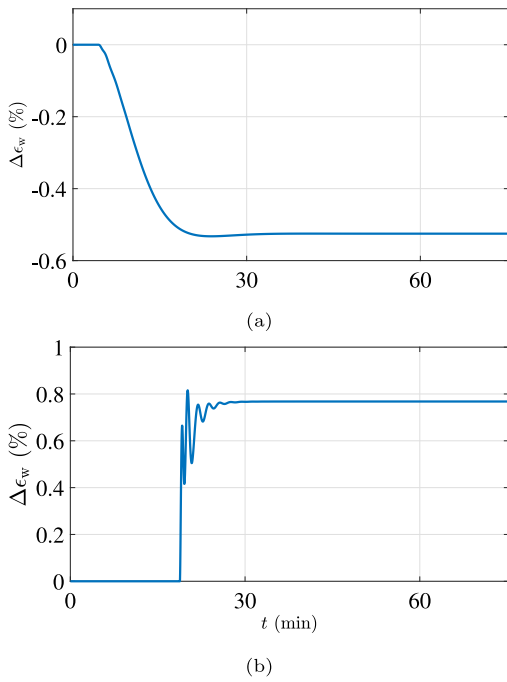
Fig. 8. Step response of the state-space model (5) and (6): **(a):** The model response to the step control input, $u[k]$. **(b):** The model response to the step input disturbance, $w[k]$.
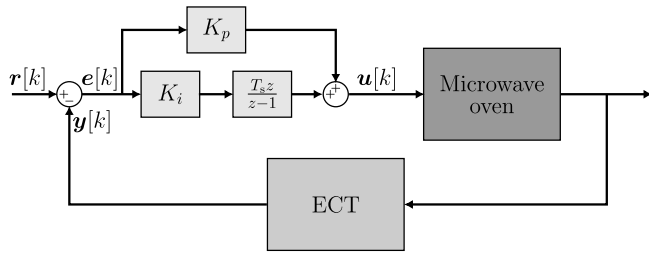

Fig. 9. The closed-loop moisture controller with the PI controller.

feedforward controller requires real-time measurements from the initial moisture and is not discussed in this paper.

In a closed-loop control with a PI controller, the average permittivity value of the output foam was estimated based on the ECT measurements, and a tracking error was calculated by comparing this value to the desired setpoint. The PI controller calculated the power levels of the magnetrons, $u[k]$, using the tracking error as

$$u[k] = \left(K_p + K_i \frac{T_s z}{z - 1} \right) e[k], \tag{7}$$

where z is a complex number in Z-transform, $e[k] = r[k] - y[k]$ is the tracking error, and $r[k]$ is the reference set point. The PI controller coefficients, K_p and K_i, are determined in MATLAB/Simulink based on several simulations with the derived model. A robust scheme was chosen to determine the controller coefficients as the process is subject to the input disturbance. The PI coefficients should be determined so that the tracking error $e[k]$ reaches zero. Moreover, the process output should not oscillate since the output oscillation in this application would mean reducing and increasing the moisture around the set point, which is not desirable. A schematic of the closed-loop control with the PI controller is shown in Fig. 9.

4.2. LQG servo control

The linear–quadratic-Gaussian (LQG) controller is a state feedback controller, which combines a linear–quadratic-regulator (LQR) and a Kalman Filter. The LQR controller has been known for its simple structure and robust properties. The preliminary application of an LQR controller for the microwave drying process was already established through simulations for one of the oven modules [23].

The standard process model to design an LQR controller is a state-space model without the input disturbance, so in the design process, it is assumed that $w[k] = 0$. Furthermore, there cannot be any time delay for the control input. A standard method to convert a discrete-time system with an input delay of T_{d1} sampling periods to a system without delay is adding T_{d1} poles at $z = 0$. This way, after absorbing the input time delay and omitting the input disturbance, the process model (5) can be stated as

$$x_{nd}[k + 1] = A_{nd} x_{nd}[k] + B_{1,nd} u[k], \tag{8}$$

where $x_{nd} \in \mathbb{R}^{269 \times 1}$ is the state vector of the system without delay (the order of the system is increased by $T_{d1} = 261$), and

$$A_{nd} = \begin{bmatrix} A & B_1 & 0_{8 \times 260} \\ 0_{260 \times 8} & 0_{260 \times 1} & I_{260 \times 260} \\ 0 & 0 & 0 \end{bmatrix} \tag{9}$$

$$B_{1,nd} = \begin{bmatrix} 0_{1 \times 268} & 1 \end{bmatrix}^T. \tag{10}$$

The LQR controller calculates $u[k]$ based on solving an optimization problem subject to the system (8) such that the state vector of the system, $x_{nd}[k]$, converges to zero (the equilibrium point). However, since the control objective is to follow a reference set point, the integral of the tracking error $e[k]$ is augmented with the state vector $x_{nd}[k]$ to form an augmented system with the state vector $\eta[k] = \begin{bmatrix} x_{nd}^T[k] & x_i^T[k] \end{bmatrix}^T$ where $x_i[k + 1] = x_i[k] + T_s (r[k] - y[k])$ is the integral of $e[k]$.

The LQR controller can be designed for the augmented system as $u[k] = -K \eta[k]$ to minimize the cost function

$$J(u[k]) = \sum_{k=0}^{\infty} \left(\eta[k]^T Q \eta[k] + u[k]^T R u[k] \right), \tag{11}$$

where $R > 0$ and $Q \geq 0$ are weighting matrices, and the control gain, K, can be calculated by solving an algebraic Ricatti equation [31,32]. The control law $u[k] = -K \eta[k]$ ensures both $x_{nd}[k]$ and $x_i[k]$ converge to zero, and as a result, the system output $y[k]$ converges to the reference set point $r[k]$.

The limitation of the LQR controller is that the state vector $x_{nd}[k]$ should be available through measurements, which is not possible in most cases. More specifically, the states in state-space models derived using system identification approaches (black-box modeling) are not related to physical quantities, so they are not measurable. The LQG controller includes a Kalman Filter that estimates the state vector. The LQR controller gain can then be multiplied by the state estimates rather than their actual measurements. Since an integral action is added to the standard LQR control, the proposed controller is called the LQG servo controller, and its schematic is shown in Fig. 10.

The Kalman filter can estimate the system state vector having the system input and output. The process model formulation for designing the Kalman filter takes into account the input disturbance and the measurement noise and can be stated as

$$x_{nd}[k + 1] = A_{nd} x_{nd}[k] + B_{1,nd} u[k] + B_{2,nd} w_{nd}[k] \tag{12}$$

$$y[k] = C_{nd} x_{nd}[k] + v[k], \tag{13}$$

where $w_{nd}[k] = w[k - T_{d2}]$ is the delayed input disturbance, and $v[k]$ is the measurement noise. The input disturbance is

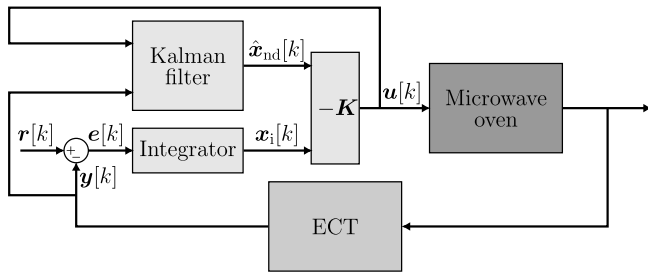**Fig. 10.** The closed-loop moisture controller with the LQG servo controller.

Fig. 11. The sample foam sheet with three separate moisture locations used for evaluating the ECT sensor performance.

measurable and available T_{d2} sampling periods in advance. The matrices $\boldsymbol{B}_{2,nd}$ and $\boldsymbol{C}_{nd}$ are

$$\boldsymbol{B}_{2,nd} = \begin{bmatrix} \boldsymbol{B}_2^T & \boldsymbol{0}_{1\times261} \end{bmatrix}^T, \quad \boldsymbol{C}_{nd} = \begin{bmatrix} \boldsymbol{C} & \boldsymbol{0}_{1\times261} \end{bmatrix}. \tag{14}$$

Assuming

$$E(\boldsymbol{w}_{nd}[k]) = E(\boldsymbol{v}[k]) = 0 \tag{15}$$

and

$$E(\boldsymbol{w}_{nd[k]}\boldsymbol{w}_{nd}^T[k]) = \boldsymbol{\Gamma}_w, \ E(\boldsymbol{v}[k]\boldsymbol{v}^T[k]) = \boldsymbol{\Gamma}_v, \tag{16}$$

with $\boldsymbol{\Gamma}_w \geq 0$ and $\boldsymbol{\Gamma}_v > 0$, the state equation of the estimator can be written as

$$\hat{\boldsymbol{x}}_{nd}[k+1|k] = \boldsymbol{A}_{nd}\hat{\boldsymbol{x}}_{nd}[k|k-1] + \boldsymbol{B}_{1,nd}\boldsymbol{u}[k] +$$
$$\boldsymbol{L}\left(\boldsymbol{y}[k] - \boldsymbol{C}_{nd}\hat{\boldsymbol{x}}_{nd}[k|k-1]\right), \tag{17}$$

where $\boldsymbol{L}$ is the Kalman Filter gain that is calculated by solving an algebraic Riccati equation [33,34].

5. Results and discussion

5.1. Experimental results of ECT

Several experiments were carried out to evaluate the performance of the ECT sensor in identifying the moisture locations and the moisture content in polymer foams. Fig. 11 shows a foam sheet used in one of these experiments. To validate the ECT reconstruction results, three pieces of this foam sheet labeled with P1, P2, and P3, were cut, moisturized with different amounts of water, and returned to their original locations. The foam sheet was inserted inside the ECT sensor while the three moisture locations were located between the top and bottom electrode planes.

The ECT sensor measured the inter-electrode capacitances of the electrodes while the wet foam was inside the sensor. As explained in Section 2, another set of measurements was also obtained with the dry foam and used as the reference in the reconstruction algorithm. Fig. 12 illustrates the measured capacitances for both the wet and dry foams. As can be seen, most of the measured capacitance values are higher in the wet foam than the dry foam due to the presence of water.

The ECT reconstruction algorithm computed the 2D permittivity change ($\Delta\epsilon$) distribution of the foam cross-section. Fig. 13 shows the reconstructed permittivity change, while the red rectangles illustrate the actual moisture locations. As can be seen, all three moisture locations are identified with good accuracy, and the difference in their moisture content can be recognized. As explained in Section 2, the permittivity change is correlated with moisture percentage, so using the calibration curve given in [21], the moisture distribution can be recovered from the permittivity estimate. The average relative estimation error in these experiments was 7.6%, which indicates a good accuracy
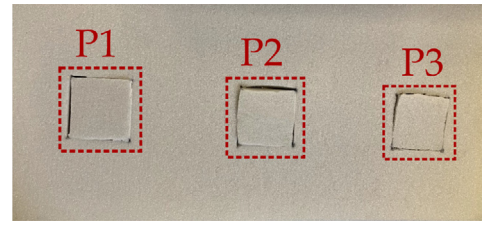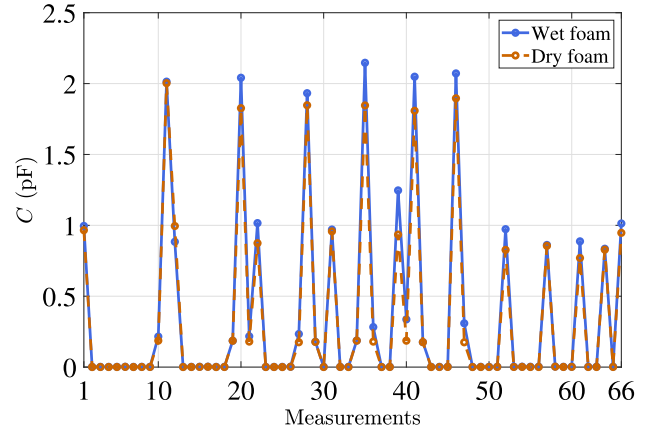

Fig. 12. Measured capacitance data with wet and dry foams.

for the designed ECT sensor [21]. However, the proposed control strategy in this study only uses the permittivity change of the foam, and the calibration for the moisture is not employed since it will result in additional calibration errors.

5.2. Experimental results of process modeling

A series of continuous microwave drying experiments were conducted to collect enough input and output data to find a process model using the system identification approaches. In the experiments done for this study in the HEPHAISTOS laboratory, the impregnation tub was filled with only water, and no chemical was used. The foam sheets were first dipped into the impregnation tub and passed through the rotating bars to get wet with a moisture percentage of around 70% on a wet basis. Then the weight of each foam sheet was recorded before and after the drying process using a digital scale to calculate the actual average moisture percentage on a wet basis as

$$M_{in/out} = \frac{W_w - W_d}{W_w} \times 100, \tag{18}$$

where M_{in} is the initial moisture, M_{out} is the output moisture, W_d indicates the weight of the dry foam, and W_w is the weight of the foam with moisture.

After the moisturizing process, the foam sheets were passed through the microwave oven on a conveyor belt. The ECT sensor measured the inter-electrode capacitances while the dried foam was passing through the sensor. The measurements were transferred using an ethernet cable in real-time to MATLAB software installed in a PC, where the reconstruction algorithm estimated the 2D permittivity distribution of the foam.

The first measurements were done by applying a PRBS input signal as the power level of the magnetrons and collecting the ECT measurements. The collected input–output data, including the power level (P), the variation of the input moisture (ΔM_{in}),
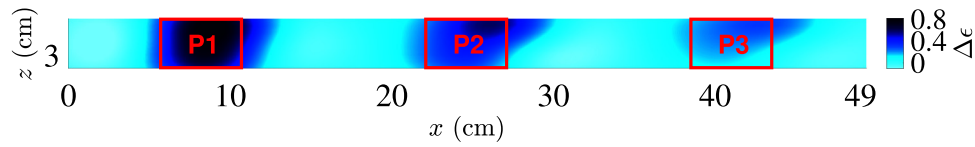
Fig. 13. The permittivity change estimation by the ECT sensor where the moisture content in P1 and P2 is almost the same (around 40%) while there is around 20% moisture present in the P3 location.

$$A = \begin{bmatrix} 1.9920 & -0.9924 & 0 & 0 & 0 & 0 & 0 & 0 \\ 1 & 0 & 0 & 0 & 0 & 0 & 0 & 0 \\ -5.799 \times 10^{-8} & 0 & 0.9987 & -0.0231 & -0.0093 & 0.0048 & -0.0077 & -9.623 \times 10^{-5} \\ -4.098 \times 10^{-8} & 0 & 0.0228 & 0.9984 & 0.0507 & 0.0011 & -0.0001 & 1.269 \times 10^{-6} \\ 2.148 \times 10^{-7} & 0 & 0.0098 & -0.0499 & 0.997 & -0.0409 & -0.0020 & 0.0002 \\ 4.097 \times 10^{-7} & 0 & -0.0047 & -0.0035 & 0.0416 & 0.9963 & 0.0753 & 9.458 \times 10^{-5} \\ -8.066 \times 10^{-8} & 0 & 0.0072 & 0.0001 & -0.0001 & -0.0754 & 0.9919 & -0.131 \\ -1.967 \times 10^{-8} & 0 & 8.531 \times 10^{-5} & 0.0008 & 0.0008 & -0.0038 & 0.0887 & 0.8314 \end{bmatrix}$$

$$B_1 = \begin{bmatrix} 2 & 0 & 0 & 0 & 0 & 0 & 0 & 0 \end{bmatrix}^T$$

$$B_2 = \begin{bmatrix} 0 & 0 & 0.0015 & 0.0021 & -0.0070 & -0.0095 & -0.0021 & -0.0012 \end{bmatrix}^T$$

$$C = \begin{bmatrix} 0 & 0 & -154.440 & -13.853 & -16.738 & -16.272 & 0.070 & 0.001 \end{bmatrix}.$$

Fig. 14. The parameters of the state-space model (5) and (6).

and the average permittivity change on a wet basis ($\Delta\epsilon_w$), were used in the MATLAB system identification toolbox to estimate the model parameters in (5) and (6). The model parameters were calculated using the least square method and are presented in Fig. 14. Fig. 15 shows the PRBS input signal, the measured output, and the model response for the same input. As can be seen, the model response follows the actual measurements.

The estimated model was validated with another dataset where an APRBS input signal was applied to the magnetrons. The applied APRBS signal, the actual ECT reconstructions, and the model response are shown in Fig. 16. As seen, although this set of data was not used in estimating the model parameters, the estimated model can estimate the system response with sufficient accuracy.

5.3. Experimental results of the proposed control methods

The PI and the LQG controllers were designed based on the derived model, and the performance of each designed controller was evaluated separately by conducting continuous drying processes. The HEPHAISTOS microwave oven is operated by software named SIMPAC developed by the manufacturing company of the microwave system, Wiess Technik GmbH, Germany. The power levels of the magnetrons can be adjusted in MATLAB software and sent to the SIMPAC through an interface connecting MATLAB and SIMPAC. Therefore, the designed PI and LQG controllers in Section 4 were implemented in MATLAB software, and they also had access to the ECT sensor measurements.

As the first controller, the PI controller was implemented to control the output foam permittivity, and the experimental results are shown in Fig. 17. The system output measured by the ECT sensor is shown in Fig. 17(a). The setpoint for the first 120 min of the experiment was 20%, while we changed it to 10% for the rest of the experiment to evaluate the performance of the
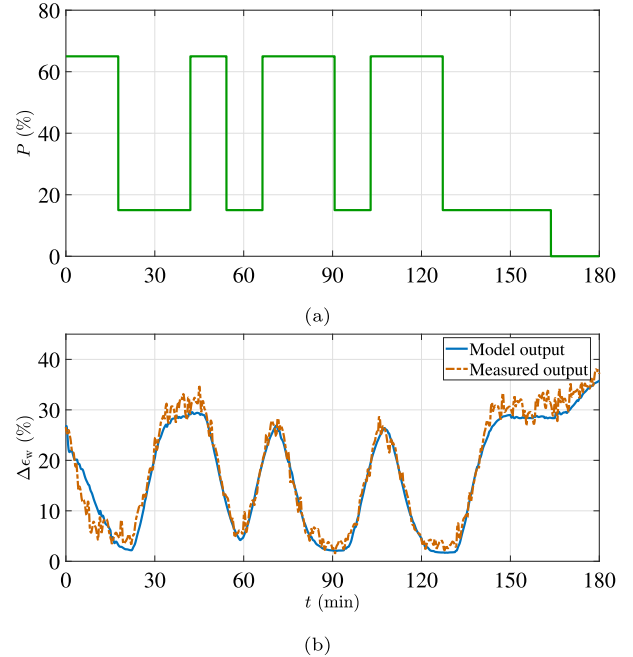

(a)

(b)

Fig. 15. The dataset with the PRBS input signal used for estimating the process model: (**a**) The applied input power percentage to the magnetrons. (**b**) The measured output and the model response for the same input.

controller in tracking a different set point. As can be seen, the process output, $\Delta\epsilon_w$, has followed the set point in both cases with reasonable accuracy. The PI controller output in this experiment which was the command power level for the magnetrons is illustrated in Fig. 17(b).
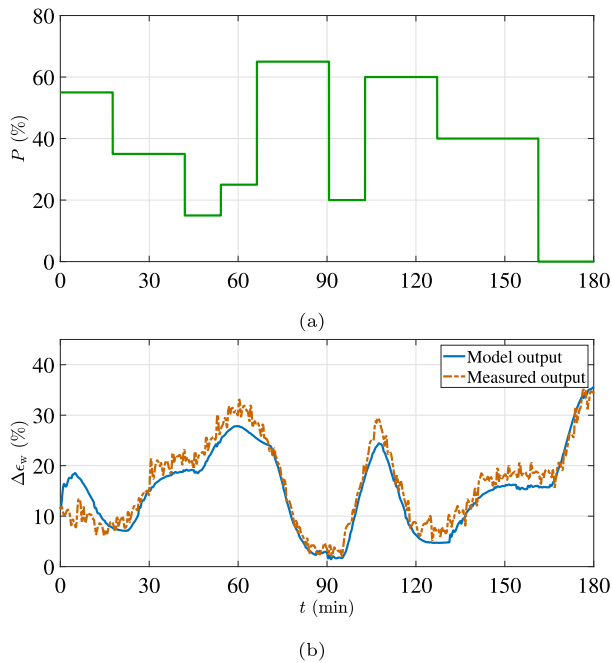
Fig. 16. The dataset with the APRBS input signal used for validating the process model: (**a**) The applied input power percentage to the magnetrons. (**b**) The measured output and the model response for the same input.
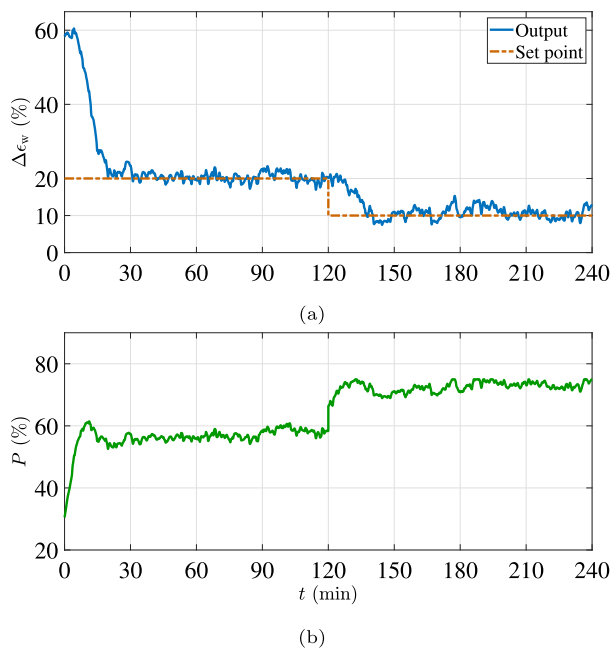

Fig. 17. The experimental results with the PI controller: (**a**): The system output while the PI controller was implemented. (**b**): The PI controller output, $u[k]$.

The absolute value of the tracking error, $e[k]$, is displayed in Fig. 18 to evaluate the controller performance better. As can be seen, the tracking error at the beginning of the experiment is significant due to the high initial moisture percentage of the foam. As time passes and the magnetrons start to work with the command power level calculated by the PI controller, the tracking error converges to near zero and remains there with some small amplitude oscillations. During the setpoint change at $t = 120$ min, the tracking error temporarily increases and then again converges to zero. The experimental results from Figs. 17
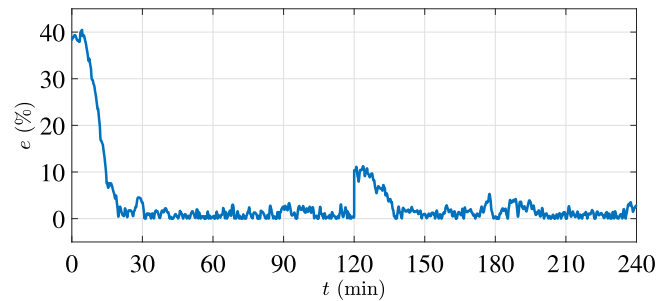

Fig. 18. The set point tracking error while the PI controller was implemented.

and 18 suggest that the designed PI controller is capable of following a reference set point with great accuracy.

The moisture percentages of the polymer foams before and after the drying process in the experiment with the PI controller are illustrated in Fig. 19. As only one average value was calculated per foam sheet, the calculated value was kept constant in these figures for 3.75 min, which corresponds to the traveling time of each foam sheet.

Fig. 19(a) shows the initial moisture, while shifted by 1129 s (around 19 min) to be synchronized with the output moisture for better presentation. The initial moisture was tried to be kept at a constant level. However, due to practical limitations, it had a variation of around 4%. As explained in Section 3.2, the variation of initial moisture was taken as the input disturbance and used in modeling the process.

The output moisture shown in Fig. 19(b) was calculated after the drying process. In practice, the ECT sensor was employed to estimate the foam permittivity correlated with moisture. The ECT estimates were calculated automatically and in real-time. However, to evaluate the ECT sensor results, the actual weight of the foam sheets was manually measured using a digital scale to compare with the ECT measurements. As seen in Fig. 19(b), the output moisture percentage has dropped with some small oscillations to an almost fixed level, which correlates with the set point permittivity of 20%. After reducing the set point permittivity to 10% at $t = 120$ min, the output moisture has also reduced to a lower steady-state value. Fig. 19 shows the good performance of the ECT sensor in estimating the permittivity (moisture) and confirms that the foam moisture after the drying process was able to follow a certain level corresponding to the set point permittivity.

As the second controller, the LQG controller was implemented for the microwave oven, and the system performance was evaluated by conducting a drying experiment. Fig. 20 shows the experimental results with the LQG controller. In this experiment, the reference set point changed from 20% to 10% at $t = 60$ min and then again from 10% to 25% at $t = 120$ min to evaluate the controller performance in tracking multiple set points. As shown in Fig. 20(a), the system output follows the set point, although it has some fluctuations.

It should be noted that the LQG controller was a linear controller that was designed for the highly nonlinear microwave system. Therefore, the modeling error coming from the linear approximation can highly affect the performance of the system. Moreover, if the initial value (moisture) is far from the set point, it may fall out of the domain of attraction, and as a result, the controller cannot guarantee the set point tracking. The results show that although a linear model was fitted to a highly nonlinear process, the controller could still follow the set point.

The corresponding power percentage with the designed LQG controller is shown in Fig. 20(b). As can be seen, the command
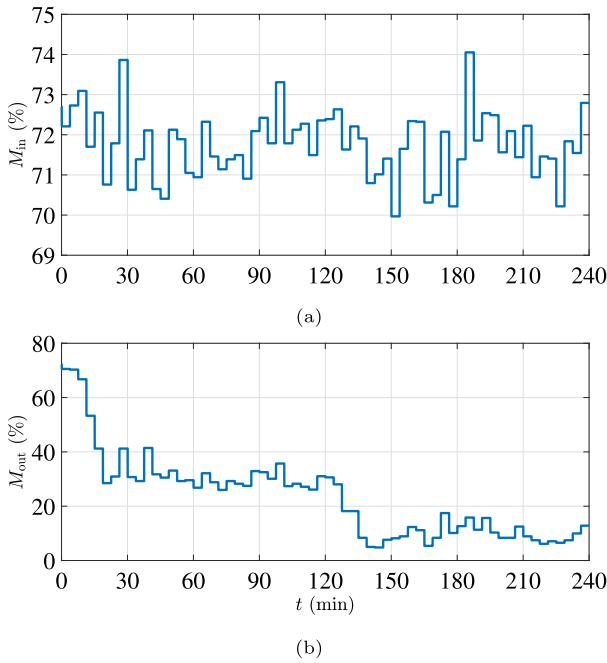
Fig. 19. The recorded moisture percentage of the polymer foams in the experiment with the PI controller **(a):** The initial moisture percentage of polymer foams before the drying process. **(b):** The moisture percentage of the polymer foams after the drying process.
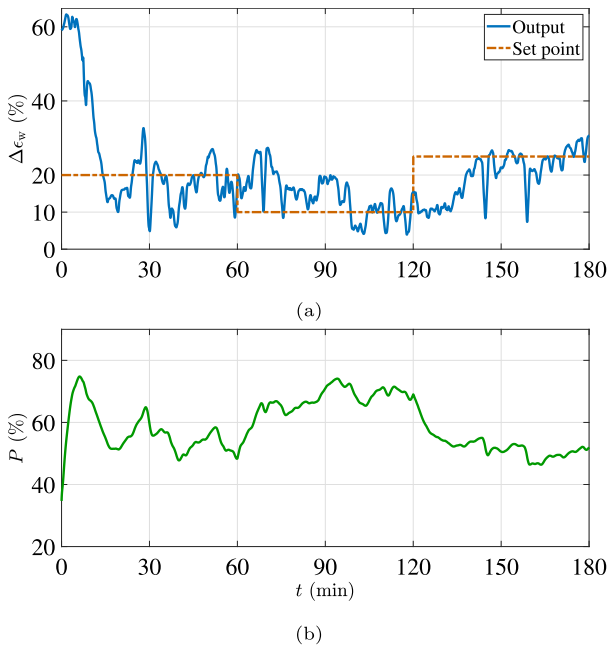

Fig. 20. The experimental results with the LQG controller: **(a):** The system output while the LQG controller was implemented. **(b):** The LQG controller output, $\boldsymbol{u}[k]$.

control calculated by the LQG controller has a smooth curve and stays within the control constraints. (It was preferable that the controller output does not exceed 75% and stays greater than 15%).

The absolute value of the tracking error in this experiment is shown in Fig. 21. The tracking error in this experiment had decreased from the start point and got close to zero. However, due to several reasons, it shows high fluctuations around zero.
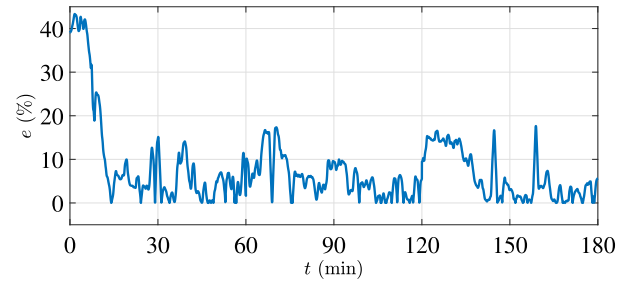

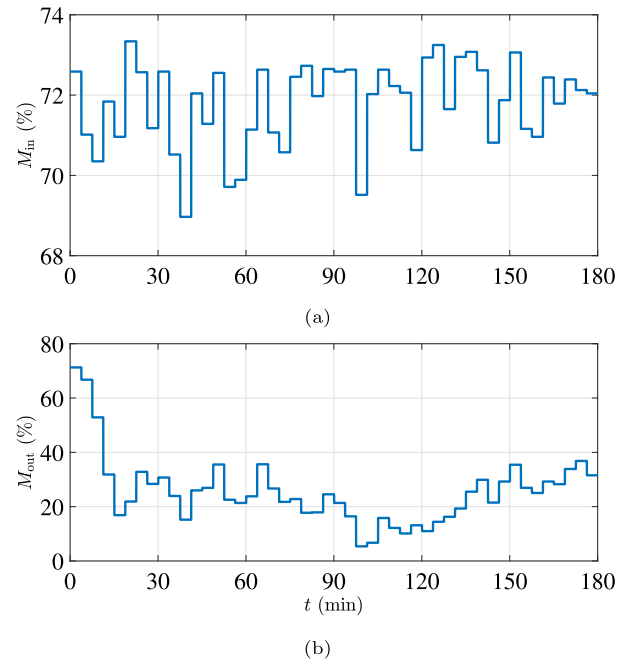**Fig. 21.** The set point tracking error while the LQG controller was implemented.

Fig. 22. The recorded moisture percentage of the polymer foams in the experiment with the LQG controller **(a):** The initial moisture percentage of polymer foams before the drying process. **(b):** The moisture percentage of the polymer foams after the drying process.

The moisture percentages of foam sheets before and after drying recorded in this experiment are shown in Fig. 22. Fig. 22(a) shows the initial moisture, while the foam moisture after the process is shown in Fig. 22(b). As can be seen in this figure, the output moisture has reduced and increased in the same intervals where the set point had changed ($t = 60$ min and $t = 120$ min).

The experiments with the PI and LQG controllers were designed with different set points and time duration, so they are not fully comparable. Furthermore, since the initial foam moisture (the input disturbance) is different in every experiment, it is not easy to compare the results. However, since the set point in the first 60 min of both experiments was 20%, the results from these experiments are compared during the first 60 min.

Fig. 23 shows the comparison between the experimental results with the PI and the LQG controllers. As seen in Fig. 23(a), the system output with the PI controller converges to the set point with lower fluctuations than the system output with the LQG controller. The average absolute value of the tracking error in the shown interval for the PI controller is 8.6%, while it is 10.5% for the LQG controller. However, the LQG controller response is faster than the PI controller, and the system output has reduced to the set point at $t = 14$ min, while with the PI controller, it has reached the set point at $t = 20$ min.
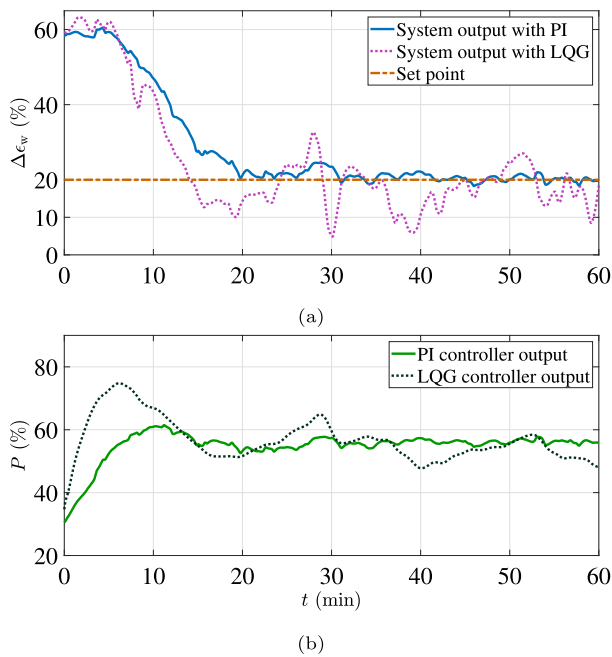
Fig. 23. The comparison between the performance of the PI and LQG controllers: **(a):** The system output with PI and LQG controller implemented. **(b):** The PI and LQG controller outputs, $\boldsymbol{u}[k]$.

Fig. 24. The simulation results with the PI controller. **(a):** The model output. **(b):** The PI controller output, $\boldsymbol{u}[k]$.

The power level calculated with each controller is shown in Fig. 23(b). The results show that at the beginning of the experiment, the LQG controller generates a larger output than the PI controller, which is the reason for its fast response. However, later the LQG controller output becomes less than the PI controller output. In general, 20.4 kWh energy was spent in the first hour of the experiment with the LQG controller, while it was slightly less for the PI controller with a total energy of 19.7 kWh.

The LQG controller had several design parameters in designing the LQR controller and the Kalman filter. The performance of the controller and the fluctuations around the set point can be enhanced by adjusting these parameters. Furthermore, the impregnation tub used for moisturizing the foams was not as reliable as the ones used in the industry, and it had only been built based on a similar concept for these experiments. Therefore, the initial moisture in foam sheets can get highly inhomogeneous as the moisturizing part is done manually. Consequently, the initial condition (the input foam moisture) could be different for the experiment with the LQG controller than the PI controller, resulting in high fluctuations with the LQG controller seen in Fig. 23(a).

5.4. Comparison of a controlled and an uncontrolled microwave drying process

The necessity of having a controller in the loop compared to an uncontrolled microwave oven can now be investigated after implementing the PI controller. As mentioned, one of the goals in the microwave drying process is to achieve specific moisture in the material. Currently, in the industry, the necessary power for the application is obtained based on trial and error experiments. Once the necessary power is found, the power level to the magnetrons is kept constant during the whole process, regardless of the possible changes.

The disadvantage of this approach is that the trial and error step can be time-consuming and expensive with wasting material and energy. 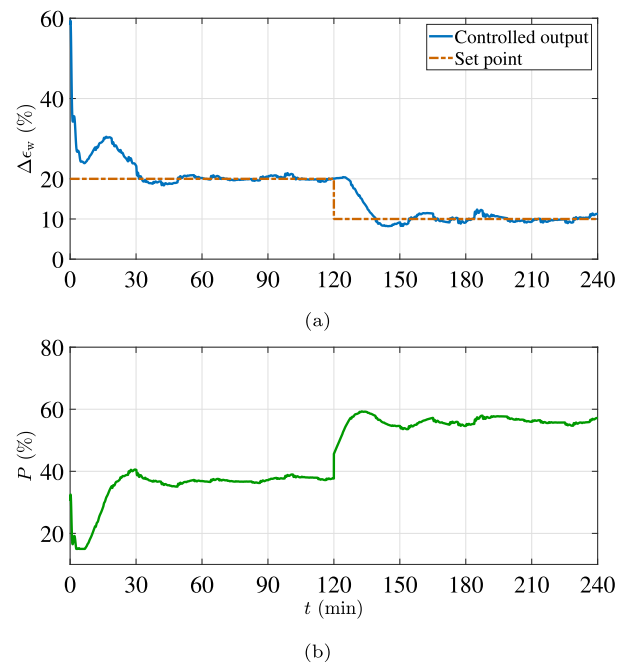Furthermore, several variables can change during the process and make it work differently than before. This approach cannot see these changes and consequently cannot act upon them. A designed moisture controller can automatically calculate the needed power based on the desired moisture. Since a feedback controller is proposed in this research, if any variable changes during the process such that it affects the system output, the controller can see the change through the changes in the ECT measurements and adjust the power levels accordingly.

A simulation study was conducted to compare the performance of the microwave drying process with and without the designed PI controller. The same scenario as the actual experiment with the PI controller was simulated with two different set points given in intervals of 120 min. The measured input moisture shown in Fig. 19(a) was used for a more accurate simulation of the actual experiment. Fig. 24 shows the simulated system output and the PI controller output in this simulation. As can be seen in Fig. 24(b), before $t = 120$ min, where the set point is 20%, the steady-state value for the power level is around 37% of the maximum power. The steady-state power level after $t = 120$ min increases to around 56% to satisfy the new set point (permittivity change of 10%). The steady-state power levels, $P_1 = 37\%$ and $P_2 = 56\%$, were calculated automatically by the PI controller based on the tracking error. Without a controller in the loop, P_1 and P_2 should be determined using the trial and error method.

Assuming that P_1 and P_2 can be found based on trial and error, these determined values cannot be accurate enough if any of the process variables change. As an example, a case was simulated where the initial moisture of the foam had dropped at some point during the simulation, a very probable situation in the drying process. Fig. 25 shows the system output with the PI controller in the loop and the system output with a constant pre-determined power level. In the constant power level case, P_1 and P_2, which were determined based on the previous simulation, were given as the input to the system in the first and the second intervals of the simulation, respectively. The initial moisture had dropped by only 5% from $t = 60$ min until the end of the simulation to compare the performance of the system in both cases.
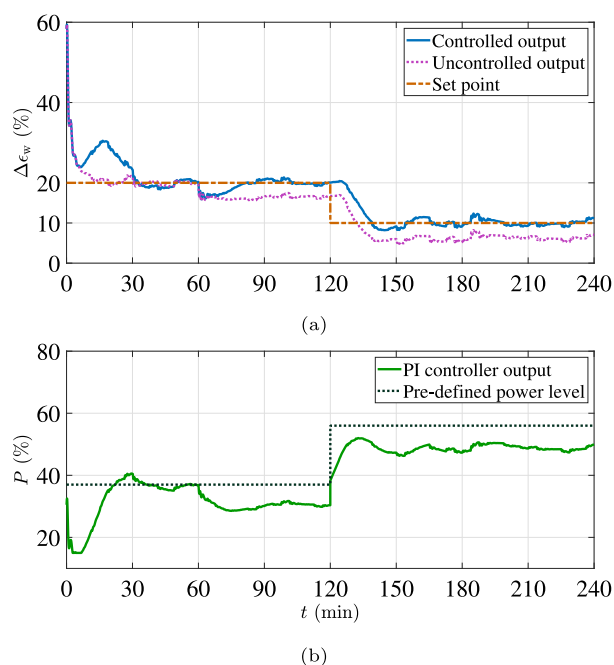
(a)

(b)

Fig. 25. The comparison of the controlled and uncontrolled simulation results with the PI controller while the initial moisture had dropped by 5% from $t = 60$ min. **(a):** The model output in the controlled and uncontrolled system. **(b):** The PI controller output, $u[k]$, and the pre-defined constant power.

As shown in Fig. 25(a), the uncontrolled system with pre-defined power level was able to follow the set point until $t = 60$ min, where the initial moisture dropped. Since the uncontrolled system cannot see the new change of the initial moisture, it kept working with the same power level as before, which resulted in reducing the material permittivity (moisture) more than the set point. In contrast, by monitoring the change in the system output, the system with the PI controller reduced the command power level after $t = 60$ min and followed the set point permittivity.

The simulation results show the importance and benefits of having a moisture controller designed for the microwave drying process. The system without the controller had resulted in an over-dry foam. The mean squared error (MSE) jumped from 6.3 to 13.0 comparing the controlled and uncontrolled system, and 9.4 kWh more energy was used during the simulation with the uncontrolled system than the controlled one (around 16% more). Note that if the initial moisture had decreased more than 5% or the duration of the experiment was more than 240 min as it is in the industry, the difference in the energy used in a controlled system compared to an uncontrolled system could be very significant.

6. Conclusion

The application of combining process tomography with control for the microwave drying process of polymer foam was investigated in this paper. The average permittivity value of the polymer foam after the drying process was controlled using two different control methods. The moisture controller received the feedback permittivity from a designed ECT sensor for this process. Furthermore, a process model with good accuracy was derived for the microwave drying process as it was a requirement for designing the controller. The moisture controller with both methods was designed using this model and implemented on the system.

Several drying experiments were conducted to evaluate the performance of the proposed control methods. The first designed controller was a PI controller, which is a popular controller in the industry. The PI controller coefficients were determined based on the simulations with the derived model such that it satisfied some criteria, including fast convergence to the set point and minimum oscillations. The experimental results showed that the PI controller had a very good performance in converging to the set point after 20 min from the beginning of the experiment, and it stayed around the set point with very low fluctuations around it. The fluctuations around the set point had an average of 9.5% of the set point.

The second controller was the LQG controller, which was designed based on the derived model. The experimental results with the LQG controller confirmed that the LQG controller could follow the set point, and the convergence time was short (14 min). However, the output had high oscillations around the set point with an average value of 31% of the set point. The observed results could be due to linear approximation errors that can highly affect the performance of the LQG controller as it is model-based. Moreover, the practical issues in moisturizing the foam at the beginning of the process can be the other possible reason. The fact that the LQG controller can still follow the set point suggests that the results could be improved by enhancing the experiment setup.

The proposed controllers can only control the average value of the permittivity distribution. In the experiment with the PI controller, when the system output was in its steady state, the permittivity change distribution was examined. Although the mean value of the permittivity change, $\Delta\epsilon_w$, was 19.9% (very close to the set point of 20%), the distribution was still inhomogeneous with some wet spots that had a maximum difference of 17.5% to the set point. In future studies, a MIMO model of the process can be derived. The aim of having a MIMO model is to use the reconstructed permittivity distribution instead of an average value and adjust the power levels of the magnetrons individually to reach homogeneous moisture in the polymer foam after the drying process.

CRediT authorship contribution statement

Marzieh Hosseini: Conceptualization, Data curation, Formal analysis, Investigation, Methodology, Software, Validation, Visualization, Writing – original draft, Writing – review & editing. **Anna Kaasinen:** Conceptualization, Supervision, Validation, Writing – review & editing. **Guido Link:** Resources, Writing – review & editing. **Mahdi Aliyari Shoorehdeli:** Validation, Writing – review & editing. **Timo Lähivaara:** Conceptualization, Writing – review & editing. **Marko Vauhkonen:** Conceptualization, Supervision, Funding acquisition, Project administration, Resources, Writing – review & editing.

Declaration of competing interest

The authors declare that they have no known competing financial interests or personal relationships that could have appeared to influence the work reported in this paper.

Acknowledgments

References

[1] P. Rattanadecho, N. Makul, Microwave-assisted drying: A review of the state-of-the-art, Drying Technol. 34 (1) (2016) 1–38.

[2] H. Zhu, T. Gulati, A.K. Datta, K. Huang, Microwave drying of spheres: Coupled electromagnetics-multiphase transport modeling with experimentation. Part I: Model development and experimental methodology, Food Bioprod. Process. 96 (2015) 314–325.

[3] L. Shen, L. Wang, C. Zheng, C. Liu, Y. Zhu, H. Liu, C. Liu, Y. Shi, X. Zheng, H. Xu, Continuous microwave drying of germinated brown rice: Effects of drying conditions on fissure and color, and modeling of moisture content and stress inside kernel, Drying Technol. 39 (5) (2021) 669–697.

[4] A. Nirmaan, B.R. Prasantha, B. Peiris, Comparison of microwave drying and oven-drying techniques for moisture determination of three paddy (Oryza sativa L.) varieties, Chem. Biol. Technol. Agric. 7 (1) (2020) 1–7.

[5] W. Cheng, G. Raghavan, M. Ngadi, N. Wang, Microwave power control strategies on the drying process II Phase-controlled and cycle-controlled microwave/air drying, J. Food Eng. 76 (2) (2006) 195–201.

[6] C. Kumar, M.U.H. Joardder, T.W. Farrell, M. Karim, Investigation of intermittent microwave convective drying (IMCD) of food materials by a coupled 3D electromagnetics and multiphase model, Drying Technol. 36 (6) (2018) 736–750.

[7] P. Chen, P.S. Schmidt, An integral model for drying of hygroscopic and nonhygroscopic materials with dielectric heating, Drying Technol. 8 (5) (1990) 907–930.

[8] B. Adu, L. Otten, Diffusion characteristics of white beans during microwave drying, J. Agric. Eng. Res. 64 (1) (1996) 61–69.

[9] Z. Li, G. Raghavan, N. Wang, C. Vigneault, Drying rate control in the middle stage of microwave drying, J. Food Eng. 104 (2) (2011) 234–238.

[10] G. Cuccurullo, L. Giordano, D. Albanese, L. Cinquanta, M. Di Matteo, Infrared thermography assisted control for apples microwave drying, J. Food Eng. 112 (4) (2012) 319–325.

[11] S. Hayden, M. Damm, C.O. Kappe, On the importance of accurate internal temperature measurements in the microwave dielectric heating of viscous systems and polymer synthesis, Macromol. Chem. Phys. 214 (4) (2013) 423–434.

[12] M.-R. Tofighi, A. Attaluri, Closed-loop pulse-width modulation microwave heating with infrared temperature control for perfusion measurement, IEEE Trans. Instrum. Meas. 70 (2020) 1–7.

[13] Y. Sun, Adaptive and Intelligent Temperature Control of Microwave Heating Systems with Multiple Sources, Vol. 8, KIT Scientific Publishing, 2016.

[14] Z. Li, G. Raghavan, V. Orsat, Temperature and power control in microwave drying, J. Food Eng. 97 (4) (2010) 478–483.

[15] A. Ruuskanen, A. Seppänen, S. Duncan, E. Somersalo, J. Kaipio, Using process tomography as a sensor for optimal control, Appl. Numer. Math. 56 (1) (2006) 37–54.

[16] M. Garcia, B. Sahovic, M. Sattar, H. Atmani, E. Schleicher, U. Hampel, L. Babout, D. Legendre, L. Portela, Control of a gas-liquid inline swirl separator based on tomographic measurements, IFAC-PapersOnLine 53 (2) (2020) 11483–11490.

[17] A. Voss, P. Hosseini, M. Pour-Ghaz, M. Vauhkonen, A. Seppänen, Three-dimensional electrical capacitance tomography–A tool for characterizing moisture transport properties of cement-based materials, Mater. Des. 181 (2019) 107967.

[18] W. Wang, K. Zhao, P. Zhang, J. Bao, S. Xue, Application of three self-developed ECT sensors for monitoring the moisture content in sand and mortar, Constr. Build. Mater. 267 (2021) 121008.

[19] P. Pan, T.P. McDonald, B.K. Via, J.P. Fulton, J.Y. Hung, Predicting moisture content of chipped pine samples with a multi-electrode capacitance sensor, Biosyst. Eng. 145 (2016) 1–9.

[20] R. Wang, M.A.R. Frias, H. Wang, W. Yang, J. Ye, Evaluation of electrical resistance tomography with voltage excitation compared with electrical capacitance tomography, Meas. Sci. Technol. 29 (12) (2018) 125401.

[21] M. Hosseini, A. Kaasinen, G. Link, T. Lähivaara, M. Vauhkonen, Electrical capacitance tomography to measure moisture distribution of polymer foam in a microwave drying process, IEEE Sens. J. 21 (16) (2021) 18101–18114.

[22] H. Feng, Y. Yin, J. Tang, Microwave drying of food and agricultural materials: basics and heat and mass transfer modeling, Food Eng. Rev. 4 (2) (2012) 89–106.

[23] M. Hosseini, A. Kaasinen, G. Link, T. Lähivaara, M. Vauhkonen, LQR Control of moisture distribution in microwave drying process based on a finite element model of parabolic PDEs, IFAC-PapersOnLine (ISSN: 2405-8963) 53 (2) (2020) 11470–11476, 21th IFAC World Congress.

[24] D. Liu, V. Kolehmainen, S. Siltanen, A.-M. Laukkanen, A. Seppänen, Nonlinear difference imaging approach to three-dimensional electrical impedance tomography in the presence of geometric modeling errors, IEEE Trans. Biomed. Eng. 63 (9) (2015) 1956–1965.

[25] A. Voss, Imaging moisture flows in cement-based materials using electrical capacitance tomography, (Ph.D. thesis), University of Eastern Finland, Department of Applied Physics, 2020.

[26] A.V. Luikov, Systems of differential equations of heat and mass transfer in capillary-porous bodies, Int. J. Heat Mass Transfer 18 (1) (1975) 1–14.

[27] D. Kocaefe, R. Younsi, B. Chaudry, Y. Kocaefe, Modeling of heat and mass transfer during high temperature treatment of aspen, Wood Sci. Technol. 40 (5) (2006) 371–391.

[28] W. Favoreel, B. De Moor, P. Van Overschee, Subspace state space system identification for industrial processes, J. Process Control 10 (2–3) (2000) 149–155.

[29] L. Fu, P. Li, The research survey of system identification method, in: 2013 5th International Conference on Intelligent Human-Machine Systems and Cybernetics, Vol.2, IEEE, 2013, pp. 397–401.

[30] M. Hosseini, A. Kaasinen, M. Aliyari Shoorehdeli, G. Link, T. Lähivaara, M. Vauhkonen, System identification of conveyor belt microwave drying process of polymer foams using electrical capacitance tomography, Sensors 21 (21) (2021) 7170.

[31] R.F. Stengel, Optimal Control and Estimation, Courier Corporation, 1994.

[32] B.D. Anderson, J.B. Moore, Optimal Control: Linear Quadratic Methods, Prentice-Hall, Inc., 1990.

[33] F.L. Lewis, F. Lewis, Optimal Estimation: With an Introduction to Stochastic Control Theory, Wiley New York, 1986.

[34] G.F. Franklin, J.D. Powell, M. Workman, Digital Control of Dynamic Systems, Second ed., Addison-Wesley Reading, MA, 1990.